Light Source Position and Reflectance Estimation from a Single View without the Distant Illumination Assumption

Kenji Hara, *Member*, *IEEE*, Ko Nishino, *Member*, *IEEE*, and Katsushi Ikeuchi, *Fellow*, *IEEE*

Abstract—Several techniques have been developed for recovering reflectance properties of real surfaces under unknown illumination. However, in most cases, those techniques assume that the light sources are located at inifinity, which cannot be applied safely to, for example, reflectance modeling of indoor environments. In this paper, we propose two types of methods to estimate the surface reflectance property of an object, as well as the position of a light source from a single view without the distant illumination assumption, thus relaxing the conditions in the previous methods. Given a real image and a 3D geometric model of an object with specular reflection as inputs, the first method estimates the light source position by fitting to the Lambertian diffuse component, while separating the specular and diffuse components by using an iterative relaxation scheme. Our second method extends that first method by using as input a specular component image, which is acquired by analyzing multiple polarization images taken from a single view, thus removing its constraints on the diffuse reflectance property. This method simultaneously recovers the reflectance properties and the light source positions by optimizing the linearity of a log-transformed Torrance-Sparrow model. By estimating the object's reflectance property and the light source position, we can freely generate synthetic images of the target object under arbitrary lighting conditions with not only source direction modification but also source-surface distance modification. Experimental results show the accuracy of our estimation framework.

Index Terms—Finite distance illumination, light source position estimation, reflectance parameter estimation, specular reflectance.

1 Introduction

Photometric modeling of real objects and their environment is an important issue in the fields of computer vision and computer graphics. It has many useful applications and one of them is augmented reality, which allows us to see a real world scene with those objects virtually and seamlessly superimposed on it. To create such realistic synthetic images, virtual objects have to be shaded consistently under the real illumination condition of the scene, which can be attained if we know the surface reflectance properties of the object and the properties of illumination including their positions. Researchers refer to this problem as the inverse rendering problem.

Several methods have been developed to simultaneously recover the surface reflectance properties and the lighting. These techniques can be divided into two categories: techniques using multiple views [13], [21], [22], [16], [17] and those using a single view [7], [29], [23], [24], [25], [11] as inputs, except 3D geometric models of the object. In the latter category, for example, Ikeuchi and Sato [7] developed an algorithm to determine both the surface reflectance properties and the light source direction from a single image based on analysis of a simplified Torrance-Sparrow reflection model [30]. Sato et al. [23], [24], [25] proposed a method for estimating the complex illumination distribution of a real scene by using a radiance distribution inside shadows cast by a real object. Tominaga and Tanaka [29] adopted the Phong model to determine the surface reflectance properties and the direction of illumination from a single color image. However, all of these methods assume that the light and viewing positions are distant, thus, they follow parallel illumination and orthogonal projection and do not offer a solution for real scene under light and viewing positions at finite distances. In general, the distant illumination assumption is not correct if the light source-surface distance is not so large, compared to the surface size, like reflectance modeling of indoor environments (Fig. 1) or photometric analysis of endoscope images [18]. One of the drawbacks of using the distant illumination assumption is when a planar surface is observed from a single view. In this case, surface normals, light directions, and viewing directions at all surface points produce the same angle. As a result, no fitting process can be applied (Fig. 2a).

Recently, a method similar to the method proposed in this paper has been introduced to recover the reflectance properties of multiple objects from a single view [1]. While we take a similar approach to separate the image into regions according to their type of reflection and fit reflection models to each regions, we will also recover the light source

- *K. Hara is with the Department of Visual Communication Design, Kyushu University, 4-9-1 Shiobaru, Minami-ku, Fukuoka 815-8540, Japan. E-mail:hara@design.kyushu-u.ac.jp.*
- *K. Nishino is with the Department of Computer Science, Columbia University, 1214 Amsterdam Avenue, MC 0401, New York, NY 10027. E-mail: kon@cs.columbia.edu.*
- *K. Ikeuchi is with the Institute of Industrial Science, The University of Tokyo, 4-6-1 Komaba, Meguro-ku, Tokyo 153-8505, Japan. E-mail: ki@cvl.iis.u-tokyo.ac.jp.*

Manuscript received 23 Nov. 2003; revised 2 Sept. 2004; accepted 5 Sept. 2004; published online 10 Feb. 2005.
Recommended for acceptance by R. Basri.
For information on obtaining reprints of this article, please send e-mail to: tpami@computer.org, and reference IEEECS Log Number TPAMI-0375-1103.

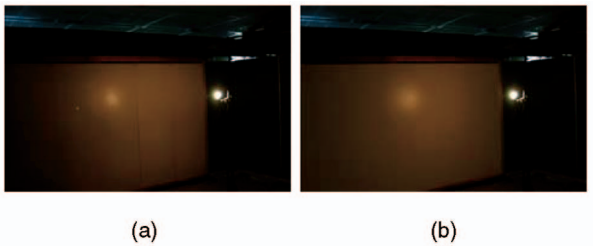

Fig. 1. An example of a synthesized image of indoor environment by estimating the surface reflectance properties: (a) real image and (b) synthesized image (the brown wall).

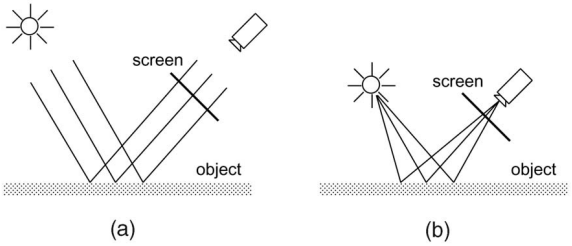

Fig 2. Illuminant and viewpoint assumptions.

position and the reflectance properties of textured surfaces with specular reflection.

Our goal is to recover the light source position and surface reflectance properties from a single view of an object captured under a single light source at a finite distance (Fig. 2b) and then create a new photo-realistic synthetic image under novel light source conditions with not only source direction modification but also light source-surface distance modification. Given a real image that has specular regions, our first method consists of two main aspects: First, we determine rough diffuse regions and the peak pixels of the whole image, which are usually located at the specular region. From these peak pixels and rough diffuse region, we initialize the values of the light source direction and source-surface distance, respectively, as well as Lambertian diffuse parameters. Then, based on these initial values, we simultaneously estimate the actual values of the light source position and reflectance properties using an iterative separating-and-fitting relaxation technique. However, this recovery method is largely limited to the following: 1) the diffuse reflection property is homogeneous Lambertian and 2) the specular peak must be visible somewhere on the surface of the target object while avoiding saturation.

We attempt to extend the above method by removing these restrictions and presenting an improved method for recovering the reflectance property and the light source position, only assuming that the target object has a homogeneous specular reflection property. First, the specular and diffuse reflection components are separated. Given the obtained component image for specular reflection (called the specular component image) and 3D geometric model of an object as an input, the second method initially estimates the light source position and the specular reflection parameters based on a linearized Torrance-Sparrow reflection model. These parameters are then refined by using the original Torrance-Sparrow reflection model.

The main advantages of our methods are: 1) it works given only a single view and a 3D geometric model of the scene and 2) unlike past methods, we estimate the three dimensional light source positions as well.

This paper is organized as follows: Section 2 describes previous work related to inverse rendering from a single view. Section 3 describes the bases necessary to our algorithm. In particular, we introduce a simplified Torrance-Sparrow reflection model that we use. Section 4 explains our first method for estimating reflectance parameters of the surface and the light source position from a real image. In Section 5, we describe our second algorithm using a specular component image as the input. Section 6 shows several results. Conclusions and future works are given in Section 7.

2 Previous Work

We discuss previous work associated with inverse rendering from a single view (recovering one or more of the surface reflectance, lighting, or texture, given a single image or multiple images taken from a single view). This section lists some of the previous research in roughly chronological order.

Pentland [19] recovers the direction of a single light source using a statistical approach, assuming a uniform distribution of the directions of the surface normals (e.g., a sphere). Ikeuchi and Sato [7] determine the specular and diffuse reflection parameters, as well as the direction of a single source from a single image and a geometric model of the object, using a simplified Torrance-Sparrow reflection model. Yang and Yuille [35] analyze the intensities and surface normals along the occluding boundaries to estimate the directions of multiple light sources. Zheng and Chellappa [37] reconstruct the shape, illuminant direction, and texture from a single image of a Lambertian surface, using shading information along image contours. Hougen and Anuja [5] determine the light source directions and its intensities from a single image of Lambertian object of known geometry by solving a set of linear equations for image irradiance. Marschner and Greenberg [11] propose a technique (called the *inverse lighting*) to reconstruct the directional distribution of light from an image of a Lambertian surface and the 3D geometric model by producing a set of basis images and finding a linear combination of those basis images that matches the input image. Kim et al. [8] estimate the illuminant direction from a single image of a Lambertian surface, while also recovering the shape of the surface, using image regions corresponding to bumps. Sato et al. [23], [24], [25] propose a method to simultaneously recover the illumination distribution (directions and intensities of light sources) and the surface reflectance by analyzing intensity information inside shadows cast on the scene by the object. Tominaga and Tanaka [29] utilize the dichromatic reflection model and the Phong model and successfully recovered the reflectance, light direction, and its color, texture, and shape under a single light source. Boivin and Gagalowicz [1] propose a method for estimating multiple reflectance properties (diffuse, specular, isotropic, and anisotropic texture) of the

different surfaces from a single image and 3D geometric model of indoor scene. Their method successively fits multiple reflection models from the simplest to the most complex and it minimizes the error between the real and synthesized images with regard to the reflection parameters. Zhang and Yang [36] detect critical points where the surface normal is perpendicular to some light source direction from a single image of a Lambertian sphere of known geometry and then determine the directions and intensities of the multiple light sources. Wang and Samaras [31] extend Zhang and Yang's method by allowing Lambertian objects of arbitrary known shapes. This approach maps the surface normals onto a sphere and then segments the surface into regions, with each region illuminated by a different set of sources. Finally, illuminant direction estimation is performed by a recursive least squares technique. Miyazaki et al. [12] present a simultaneous recovery of the shape, surface reflection, texture, and the directions of multiple sources with polarization analysis of multiple images taken from a single view. Recently, multiple cues are combined to robustly estimate the multiple directional illuminants. Wang and Samaras [32] develop a method based on shadow and a method based on shading independently and integrate the two methods. Li et al. [10] determine the directions of multiple light sources from a single image using shading, shadow, and specular reflection. This technique still works for textured surfaces.

Most of the above methods assume distant illumination (directional light sources) and then recover one or more of the direction of a single light source, directions, and intensities of multiple light sources, surface reflectance, or texture from a single image of a scene. Our method differs from these previous works in that it simultaneously estimates the position of a single light source and surface reflectance without distant illumination assumption.

3 Reflection Model

In this section, we give a brief overview on the reflection model used in our method. Generally, reflection models are described by linear combinations of two reflection components: the diffuse and the specular reflections. This model was formally introduced by Shafer [27] as the dichromatic reflection model. The diffuse reflection component represents reflected rays arising from internal scattering inside the surface medium. The specular reflection component, on the other hand, represents light rays immediately reflected on the object surface.

Specifically, we use the Torrance-Sparrow reflection model [30] by assuming that the Fresnel reflectance coefficient is constant and the geometric attenuation factor is 1. Using this reflection model, the specular reflection of an object's surface point is given as

$$I_c = \left[k_{d,c} \cos\theta_i + \frac{k_{s,c}}{\cos\theta_r} \exp\left[-\frac{\alpha^2}{2\sigma^2} \right] \right] L_c, \tag{1}$$

where index c represents R, G, and B components, I_c is the image pixel value, θ_i is the angle between the light source direction and the surface normal, θ_r is the angle between the viewing direction and the surface normal, and α is the angle between the surface normal and the bisector of the viewing direction and the light source direction (see Fig. 3). L_c is given by:

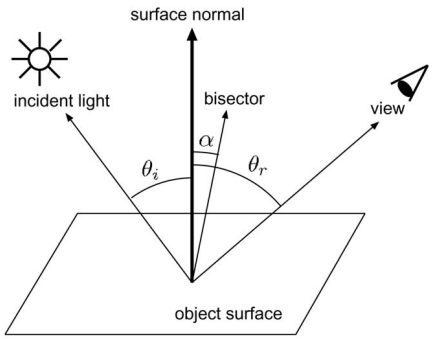

Fig. 3. Geometric model of reflection.

$$L_c = \frac{L_{q,c}}{r^2}, \tag{2}$$

where $L_{q,c}$ is the radiance of the point light source in each color band and r is the distance between the point light source and the object surface point.

$k_{d,c}$ and $k_{s,c}$ are coefficients for the diffuse and specular reflection components, respectively, and σ is the surface roughness measured as the standard deviation of microfacet orientations. In the original Torrance-Sparrow reflection model, coefficient $k_{s,c}$ contained the Fresnel reflectance coefficient F and the geometric attenuation factor G. Here, we assume that $G = 1$ and F is constant. These assumptions are valid when the viewing angle θ_r and the illuminating angle θ_i are at most 60 degrees [14].

Using a 3D geometric model and by accomplishing camera calibration, the angle θ_r can be obtained for each image pixel. Angles α and θ_i are unknown since these angles require the light source direction, which is unknown at this moment.

In (1), we can observe that the values of $(k_{d,c}, k_{s,c})$ and L_c cannot be separated by only knowing the value of I_c. Thus, we redefine the reflection parameters as:

$$K_{d,c} = k_{d,c} L_{q,c}, \quad K_{s,c} = k_{s,c} L_{q,c}. \tag{3}$$

With these definitions, we can rewrite (1) as:

$$I_c = \frac{K_{d,c} \cos\theta_i}{r^2} + \frac{K_{s,c}}{r^2 \cos\theta_r} \exp\left[-\frac{\alpha^2}{2\sigma^2} \right]. \tag{4}$$

In this paper, we refer to $\tilde{K}_s = (K_{s,R}, K_{s,G}, K_{s,B})$ and σ as the *specular reflection parameters* and $\tilde{K}_d = (K_{d,R}, K_{d,G}, K_{d,B})$ as the *diffuse reflection parameters*. Note that $\tilde{K}_d$ and $\tilde{K}_s$ contain the light source intensity $\tilde{L}_q = (L_{q,R}, L_{q,G}, L_{q,B})$. In Sections 4 and 5, we remove the subscript c, as the same computation is executed independently for each color band. If the estimated roughness parameters do not have the same value from the three color channels, we finally determine the roughness parameter by calculating an average of those values.

4 Source Position and Reflectance Recovery with Diffuse-Based Constraints

We now describe the algorithm for estimating the position of the light source and reflectance parameters from a single image and a 3-D geometric model of the object. Usually, to estimate the surface reflectance stably, e.g., [26], first, one separates reflection components and then uses a fitting algorithm to obtain the parameters. However, this approach is unfeasible for an unknown light source position. Consequently, under this condition, we can hardly make the surface reflectance and light source position estimation process completely separated. One of the strategies to solve this problem is to use a certain relaxation technique of iterative separating-and-fitting.

In this method, we assume:

1. the camera parameter is known;
2. interreflection, cast shadows, and saturated pixel values are avoided (hence, it is limited to convex objects);
3. the scene is illuminated by a single point light source;
4. at least one specular peak is visible on the surface of the target object;
5. the surface reflection can be uniformly modeled as a linear combination of the Lambertian diffuse model with constant albedo (inside K_d) and the Torrance-Sparrow specular model; and
6. the object in interest is segmented out in the image as other methods similarly assume.

4.1 Light Source Distance

The light source direction at object's surface point P satisfying $\alpha = 0$ can be written as

$$\boldsymbol{L}_p = 2(\boldsymbol{N}_p^T \boldsymbol{V}_p)\boldsymbol{N}_p - \boldsymbol{V}_p, \tag{5}$$

where $\boldsymbol{L}_p$ is a unit vector with a light source direction and a starting point P, $\boldsymbol{V}_p$ is a unit vector with a viewing direction and a starting point P, and $\boldsymbol{N}_p$ is a unit normal vector at P. $\boldsymbol{N}_p^T \boldsymbol{V}_p$ denotes the scalar product of $\boldsymbol{N}_p$ and $\boldsymbol{V}_p$ with the transpose notation T. Then, the location vector $\boldsymbol{L}$ of the light source can be expressed as

$$\boldsymbol{L} = \boldsymbol{P} + t\boldsymbol{L}_p, \tag{6}$$

where $\boldsymbol{P}$ is the location vector of P and t is the distance between $\boldsymbol{P}$ and $\boldsymbol{L}$.

We can regard the specular peak (i_p, j_p) as the pixel location of P. Because of the off-specular peak, the point P will not be the specular peak. However, it will be plenty close for practical purposes except at grazing angles. As a consequence, once we obtain (i_p, j_p), $\boldsymbol{P}$ can be calculated using the camera projection matrix, which is $\boldsymbol{L}_p$ directly computable from (5). However, to estimate the light source position, we also need the value of t (the light source distance), which is unknown.

In the next section, we describe how to estimate t and the reflectance parameters in (4) simultaneously.

4.2 Model Fitting to Lambertian Diffuse Component

To obtain the initial guesses of the light source distance and reflectance parameters, we need the following two steps: First, we extract the diffuse region Ω_d

$$\Omega_d = \left\{(i,j) \in \Omega \mid (i-i_p)^2 + (j-j_p)^2 > T^2\right\}, \tag{7}$$

where Ω is the set of 2D points of object's surface points and T is a positive integer concerning the radius of the specular region. In many cases, it is difficult to automatically identify the optimal value of T without any knowledge of the surface roughness σ which is to be estimated. Therefore, we manually specify the value of T. However, as our method uses an alternating procedure of simultaneously estimating the diffuse and specular reflection components, the final result does not depend largely upon the value of T (as described later in Section 5.3). Then, we determine the light source distance t by fitting the diffuse term of (4) to the diffuse region, which means

$$t^* = \underset{t}{\operatorname{argmin}} \sum_{(i,j)\in\Omega_d} \left[u(i,j,t) - \frac{1}{N_d} \sum_{(i,j)\in\Omega_d} u(i,j,t) \right]^2, \tag{8}$$

where Ω_d and N_d are the set and the number of the 2D points in the diffuse region image, $u(i,j,t)$ is defined as

$$u(i,j,t) = \frac{I(i,j) r(i,j,t)^2}{\cos\theta_i(i,j,t)}, \quad (i,j) \in \Omega_d, \tag{9}$$

where $I(i,j)$ is the pixel value observed at 2D point (i,j) in the original image, $r(i,j,t)$ is the distance between the light source and the surface point of 2D point (i,j) under the light source distance t, and $\theta_i(i,j,t)$ is the incident angle at this surface point.

Since (8) is difficult to be solved analytically, we search the optimal source distance t^* in the finite, discrete solution space $\Omega_t = \{t_{min}, t_{min} + \Delta t, \ldots, t_{max} - \Delta t, t_{max}\}$, where t_{min}, t_{max}, and Δt are the user-defined lower bound, upper bound, and step length with respect to t, respectively. The step length Δt should be chosen comparable to or larger than the sampling interval (spatial resolution) R of the input image ($\Delta t / R \gtrsim 1$).

Second, we estimate the diffuse reflection parameters K_d using t^* by minimizing the squared error as

$$K_d^* = \underset{K_d}{\operatorname{argmin}} \sum_{(i,j)\in\Omega_d} \left(I(i,j) - \frac{K_d \cos\theta_i(i,j,t^*)}{r(i,j,t^*)^2} \right)^2. \tag{10}$$

The solution K_d^* can be expressed as

$$K_d^* = \frac{\sum_{(i,j)\in\Omega_d} I(i,j)}{\sum_{(i,j)\in\Omega_d} \frac{\cos\theta_i(i,j,t^*)}{r(i,j,t^*)^2}}. \tag{11}$$

4.3 Separating-and-Fitting Iterative Relaxation Refinement

The specular component of the input image can be obtained by subtracting the aforementioned diffuse estimate from the

input image. The pixel value at point (i,j) in the specular image can be computed as

$$I_s^*(i,j) = I(i,j) - \frac{K_d^* \cos\theta_i(i,j,t^*)}{r(i,j,t^*)^2}, \quad (i,j) \in \Omega. \tag{12}$$

To accomplish fitting the specular reflection model to the residual image I_s^*, we need to solve a nonlinear optimization problem as

$$\underset{K_s,\sigma}{\operatorname{argmin}} \sum_{(i,j)\in\Omega} \left(I_s^*(i,j) - \frac{K_s}{r(i,j,t^*)^2 \cos\theta_r(i,j)} \times \exp\left[-\frac{\alpha(i,j,t^*)^2}{2\sigma^2}\right]\right)^2. \tag{13}$$

To obtain desirable solutions, we use a two-step algorithm. The detail is as follows.

4.3.1 Initial Estimation of (K_s, σ):

We rewrite the specular reflection model as

$$I_s(i,j,t) = \frac{K_s}{r(i,j,t)^2 \cos\theta_r(i,j)} \exp\left[-\frac{\alpha(i,j,t)^2}{2\sigma^2}\right], \quad (i,j) \in \Omega. \tag{14}$$

In order to solve (13), the following equation can be derived by the logarithmic transformation of (14):

$$y(i,j) = -\frac{1}{\sigma^2} x(i,j) + \ln K_s \ (i,j) \in \Omega, \tag{15}$$

where

$$x(i,j) = \frac{\alpha(i,j,t^*)^2}{2}, \tag{16}$$

$$y(i,j) = \ln\left[I_s^*(i,j) r(i,j,t^*)^2 \cos\theta_r(i,j)\right], \tag{17}$$

by which we can plot a set of data pairs $(x(i,j), y(i,j))$, $(i,j) \in \Omega$. By line fitting on these 2D points based on a least-squares method, and then by comparing the coefficients of the regression line with (15), we obtain the initial estimates K_s^* and σ^* of the specular reflection parameters as

$$K_s^* = \exp(b), \tag{18}$$

$$\sigma^* = \sqrt{-\frac{1}{a}}, \tag{19}$$

where $a < 0$ and b are, respectively, the slope and Y-intercept of the least-squares regression line.

4.3.2 Refinement of (K_s, σ):

The estimated specular reflection parameters in the first step is based on the logarithm fitting, thus the synthesized image based on the initial estimates (K_s^*, σ^*) is still quite different from the input image. In this step, we search for the solution of (13) locally around the initial guesses (K_s^*, σ^*) through a two-fold iteration algorithm as follows:

Algorithm `updating rule for` (K_s, σ)

1. Set iteration count $k \leftarrow 0$. Set $K_s^{(0)} \leftarrow K_s^*$. Set $\sigma^{(0)} \leftarrow \sigma^*$. Set $I_s^*(i,j) \leftarrow I(i,j) - \frac{K_d^* \cos\theta_i(i,j,t^*)}{r(i,j,t^*)^2}$. Repeat Step 2$\sim$ Step 4 until convergence.
2. $$K_s^{(k+1)} \leftarrow \frac{\sum_{(i,j)\in\Omega} I_s^*(i,j)}{\sum_{(i,j)\in\Omega} \frac{1}{r(i,j,t^*)^2 \cos\theta_r(i,j)} \exp\left[-\frac{\alpha(i,j,t^*)^2}{2(\sigma^{(k)})^2}\right]}.$$
3. Set iteration count $l \leftarrow 0$. Set $\mu^{(0)} \leftarrow \frac{1}{\sigma^{(k)}}$. Repeat Step 3a $\sim$ Step 3b until convergence.
   a. $$\mu^{(l+1)} \leftarrow \mu^{(l)} - \gamma \sum_{(i,j)\in\Omega} \left[\left(I_s^*(i,j) - \frac{K_s^{(k+1)}}{r(i,j,t^*)^2 \cos\theta_r(i,j)} \exp\left[-\frac{\alpha(i,j,t^*)^2 (\mu^{(l)})^2}{2}\right]\right)^2 \times \frac{K_s^{(k+1)} \alpha(i,j,t^*)^2 \mu^{(l)}}{r(i,j,t^*)^2 \cos\theta_r(i,j)} \exp\left[-\frac{\alpha(i,j,t^*)^2 (\mu^{(l)})^2}{2}\right]\right].$$
   b. $l \leftarrow (l+1)$.
4. $\sigma^{(k+1)} \leftarrow \frac{1}{\mu^{(l)}}$, $k \leftarrow (k+1)$.
5. $K_s^* \leftarrow K_s^{(k)}$, $\sigma^* \leftarrow \sigma^{(k)}$.

Note that the optimum value of γ has to be chosen carefully (if it is too small, it is slow to converge; if too large, oscillations may occur). In this paper, γ has been experimentally chosen small ($\gamma = 1.0 \times 10^{-7}$) enough so that the iterates converge safely. Typically, for the input synthetic image in Fig. 6, the above algorithm took 25 iterations and 3 minutes to converge.

Using the above algorithm, we can obtain the estimates (K_s^*, σ^*) of the specular reflection parameters. However, $(K_d^*, K_s^*, \sigma^*, t^*)$ are still inaccurate since they are computed based only on the rough diffuse regions. Therefore, we have to update the diffuse reflection component, as described in the following equations:

$$I_d^*(i,j) = I(i,j) - \frac{K_s^*}{r(i,j,t^*)^2 \cos\theta_r(i,j)} \exp\left[-\frac{\alpha(i,j,t^*)^2}{2(\sigma^*)^2}\right], \quad (i,j) \in \Omega. \tag{20}$$

After that, we reestimate the light source distance and diffuse reflection parameters based on the following equation.

$$\underset{K_d,t\in\Omega_t}{\operatorname{argmin}} \sum_{(i,j)\in\Omega} \left(I_d^*(i,j) - \frac{K_d \cos\theta_i(i,j,t)}{r(i,j,t)^2} \right)^2. \tag{21}$$

We can solve (21) through an iteration algorithm as follows:

Algorithm `updating rule for` (K_d, t)

1. Set iteration count $k \leftarrow 0$. Set $K_d^{(0)} \leftarrow K_d^*$. Set $t^{(0)} \leftarrow t^*$. Set $I_d^*(i,j) \leftarrow I(i,j) - \frac{K_s^*}{r(i,j,t^*)^2 \cos\theta_r(i,j)} \times \exp\left[-\frac{\alpha(i,j,t^*)^2}{2(\sigma^*)^2}\right]$. Repeat Step 2 $\sim$ Step 4 until convergence.

2.
$$K_d^{(k+1)} \leftarrow \frac{\sum_{(i,j)\in\Omega} I_d^*(i,j)}{\sum_{(i,j)\in\Omega} \frac{\cos\theta_i(i,j,t^{(k)})}{r(i,j,t^{(k)})^2}}.$$

3.
$$t^{(k+1)} \leftarrow \underset{t\in\Omega_t}{\operatorname{argmin}} \sum_{(i,j)\in\Omega} \left(I_d^*(i,j) - \frac{K_d^{(k+1)}\cos\theta_i(i,j,t)}{r(i,j,t)^2}\right)^2.$$

4. $k \leftarrow (k+1)$.

5. $K_d^* \leftarrow K_d^{(k)}$, $t^* \leftarrow t^{(k)}$.

Typically, for the input synthetic image in Fig. 6, the above algorithm took 20 iterations and 8 minutes to converge. Finally, the above two algorithms are repeated alternately until the reflectance parameters and light source position become no longer changed in values or until they reach the maximum number of iterations. Using t^*, we can obtain the light source position $\boldsymbol{L}^*$ by using (6).

5 Source Position and Reflectance Recovery without Diffuse-Based Constraints

A major limitation of the algorithm of the last section is its homogeneous Lambertian approximation of the diffuse reflection. In order to avoid this restriction, our second method takes as input a specular component image instead of a real image except a 3D geometric model of an object. Also, the first technique assumed that the specular peak can be identified, though invisible specular peaks or saturated pixels are not uncommon. We also remove this constraint in the second method. In this method, we assume 1) the camera parameter is known, 2) interreflection and cast shadows are avoided (hence, it is limited to convex objects), and 3) the specular reflectance property can be uniformly modeled according to the Torrance-Sparrow model.

Using the specular reflection component, the algorithm for initially estimating the light source position, as well as the specular reflectance properties, is explained in Section 5.1. We describe the refinement of their estimated values in Section 5.2. As for the case of textured surfaces, including specular reflecion, we describe how to determine the diffuse reflection parameters in Section 5.3.

5.1 Recovery Based on Log-Linearized Torrance-Sparrow Model

In this section, we explain how to estimate the specular reflectance parameters as well as the source position from a specular component image. As stated in Section 4.1, a three dimensional source position is represented here by a twofold set $\langle p,t\rangle$, where $p=(i_p,j_p)$ is the image pixel location of the specular peak satisfying $\alpha=0$ and t is the source distance. The source position is discretized in the solution space $\langle p,t\rangle$ with a Cartesian product $\Omega_p\times\Omega_t$, where Ω_p and Ω_t are the user-defined finite, discrete search spaces with regard to p and t, respectively. At this stage, we search for the optimal values of $\langle p,t\rangle$ by a discrete optimization technique, whereas the method of Section 4 does only the source distance t for a fixed p.

Assuming that $\langle p,t\rangle$ is unknown, the linearized reflection model can be obtained based on the logarithmic transformation described in Section 4.3 as:

$$Y(i,j,p,t) = -\frac{1}{\sigma^2}X(i,j,p,t) + \ln K_s, \quad (i,j)\in\Omega, \tag{22}$$

where

$$X(i,j,p,t) = \frac{\alpha(i,j,p,t)^2}{2}, \tag{23}$$

$$Y(i,j,p,t) = \ln\left[I_s(i,j)r(i,j,p,t)^2\cos\theta_r(i,j)\right]. \tag{24}$$

Based on (22), our basic idea is to find $\langle p^+,t^+\rangle$ that yields the strongest negative linear relationship between $X(i,j,p,t)$ and $Y(i,j,p,t)$ by minimizing a correlation coefficient as

$$\underset{(p,t)\in\Omega_p\times\Omega_t}{\operatorname{argmin}} \left[\frac{\sum_{(i,j)\in\Omega}\left(X(i,j,p,t)-\overline{X}(p,t)\right)\left(Y(i,j,p,t)-\overline{Y}(p,t)\right)}{\sqrt{\sum_{(i,j)\in\Omega}\left(X(i,j,p,t)-\overline{X}(p,t)\right)^2}\sqrt{\sum_{(i,j)\in\Omega}\left(Y(i,j,p,t)-\overline{Y}(p,t)\right)^2}}\right], \tag{25}$$

where $\overline{X}(p,t)$ and $\overline{Y}(p,t)$ are sample means:

$$\overline{X}(p,t) = \frac{1}{N}\sum_{(i,j)\in\Omega} X(i,j,p,t), \tag{26}$$

$$\overline{Y}(p,t) = \frac{1}{N}\sum_{(i,j)\in\Omega} Y(i,j,p,t), \tag{27}$$

where N is the number of the 2D points belonging to Ω.

To solve (25), we apply a similar discretization approach to the one mentioned in Section 4.2. Once the optimal solution (p^+,t^+) is obtained, the specular reflection parameter (K_s^+,σ^+) can be calculated from (18) and (19). The important thing to note here is that higher t, as well as higher σ, generates a more blurred specular reflection (t is the light source distance and σ is the surface roughness) and, hence, (t,σ) seems not to be determined uniquely from only a specular component image, which makes this inverse problem ill-conditioned or ill-posed. However, in practice, t (and, therefore, also σ) can be determined uniquely from a given specular component image, as shown in the appendix.

5.2 Three-Step Numerical Optimization

Figs. 17 and 18 in the Appendix show the correlation coefficients with regard to variations of the light source distance t for different angles. Estimates of t (and, hence, also p, K_s, and σ) obtained using the method in the last section can deviate from the true values under the influence of noise, as shown in Fig. 18. In this stage, we formulate a nonlinear optimization problem with respect to K_s, σ , p, and t as:

$$\underset{K_s,\sigma,(p,t)\in\Omega_p\times\Omega_t}{\operatorname{argmin}} \sum_{(i,j)\in\Omega} \left(I_s(i,j) - \frac{K_s}{r(i,j,p,t)^2 \cos\theta_r(i,j)} \times \exp\left[-\frac{\alpha(i,j,p,t)^2}{2\sigma^2}\right]\right)^2, \tag{28}$$

where r and α are redefined as functions of (i,j,p,t). Since finding the least squares solution (28) is equivalent to maximizing the likelihood, we are able to handle independent Gaussian noise in addition to the true value at each pixel which well approximates practical camera noise. To solve (28), we apply a 3-step iterative algorithm using $(K_s^+, \sigma^+, p^+, t^+)$ as the initial guess. The procedure is described in the following:

Algorithm `updating rule for` (K_s, σ, p, t)

1. Set iteration count $k \leftarrow 0$. Set $K_s^{(0)} \leftarrow K_s^+$. Set $\sigma^{(0)} \leftarrow \sigma^+$. Set $p^{(0)} \leftarrow p^+$. Set $t^{(0)} \leftarrow t^+$. Repeat Step 2 $\sim$ Step 5 until convergence.
2. $$K_s^{(k+1)} \leftarrow \frac{\sum_{(i,j)\in\Omega} I_s(i,j)}{\sum_{(i,j)\in\Omega} \frac{1}{r(i,j,p^{(k)},t^{(k)})^2 \cos\theta_r(i,j)} \exp\left[-\frac{\alpha(i,j,p^{(k)},t^{(k)})^2}{2(\sigma^{(k)})^2}\right]}.$$
3. Set iteration count $l \leftarrow 0$. Set $\mu^{(0)} \leftarrow \frac{1}{\sigma^{(k)}}$. Repeat Step 3a $\sim$ Step 3b until convergence.
   a. $$\mu^{(l+1)} \leftarrow \mu^{(l)} - \gamma \sum_{(i,j)\in\Omega} \left[\left(I_s(i,j) - \frac{K_s^{(k+1)}}{r(i,j,p^{(k)},t^{(k)})^2 \cos\theta_r(i,j)} \times \exp\left[-\frac{\alpha(i,j,p^{(k)},t^{(k)})^2 (\mu^{(l)})^2}{2}\right]\right)^2 \times \frac{K_s^{(k+1)} \alpha(i,j,p^{(k)},t^{(k)})^2 \mu^{(l)}}{r(i,j,p^{(k)},t^{(k)})^2 \cos\theta_r(i,j)} \exp\left[-\frac{\alpha(i,j,p^{(k)},t^{(k)})^2 (\mu^{(l)})^2}{2}\right]\right].$$
   b. $l \leftarrow (l+1)$.
4. $\sigma^{(k+1)} \leftarrow \frac{1}{\mu^{(l)}}$.
5. $$(p^{(k+1)}, t^{(k+1)}) \leftarrow \underset{(p,t)\in\Omega_p\times\Omega_t}{\operatorname{argmin}} \sum_{(i,j)\in\Omega} \left(I_s(i,j) - \frac{K_s^{(k+1)}}{r(i,j,p,t)^2 \cos\theta_r(i,j)} \exp\left[-\frac{\alpha(i,j,p,t)^2}{2(\sigma^{(k+1)})^2}\right]\right)^2,$$ $k \leftarrow (k+1)$.
6. $K_s^+ \leftarrow K_s^{(k)}, \sigma^+ \leftarrow \sigma^{(k)}, p^+ \leftarrow p^{(k)}, t^+ \leftarrow t^{(k)}$.

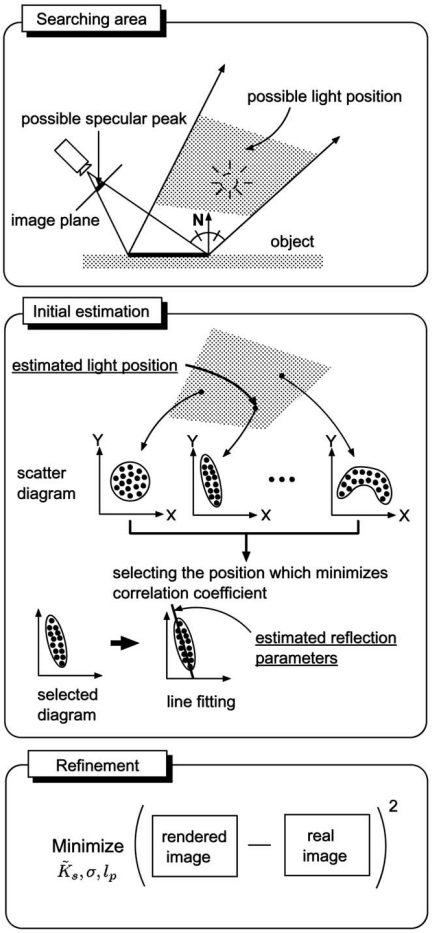

Fig. 4. Basic steps of the proposed method.

Typically, for the input synthetic image in Fig. 7, the above algorithm took 100 iterations and 20 minutes to converge. We show the outline of the overall algorithm in Fig. 4.

5.3 Diffuse Reflection Parameter Estimation

Unlike the method of Section 4, the method of this section does not directly estimate the diffuse reflection parameters. However, to synthesize new images under novel illumination conditions, we need to determine those values according to some appropriate diffuse reflection model. In the case of textured surfaces with specular reflection, we determine the Lambertian reflectance parameters for each pixel, i.e., texture, as

$$K_d^+(i,j) = \frac{r(i,j,p^+,t^+)^2 I_d(i,j)}{\cos\theta_i(i,j,p^+,t^+)}, \quad (i,j)\in\Omega, \tag{29}$$

where I_d is the separated diffuse component image and θ_i is the incident angle. p^+ and t^+ are, respectively, the estimated specular peak and light source distance in the last subsection. Note that shadowing is not considered in our method.

6 Experiments

In this section, we present results of several experiments using synthetic and real images. First, the experiments

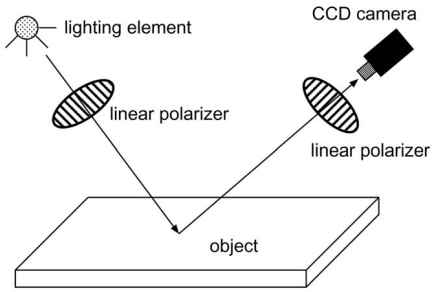

Fig. 5. Experimental setup.

using synthetic images demonstrate that our methods can use the simplified Torrance-Sparrow reflection model to correctly estimate the light source position even if the observed image is generated under a more complex reflection model. In these experiments, we generate the input synthetic image using RADIANCE [20] as rendering software Note that RADIANCE employs Ward's BRDF model [33].

Next, the experiments using real images aim to show the applicability of our methods to real problems. The sizes of the objects used in the experiments are approximately the same as a 15cm cube (each fits into a cube 15cm on a side) and the light source is not very far (the light source distance: 80cm-100cm). Color images are captured using a color CCD video camera and 3D geometric models are obtained using a light-stripe range finder with a liquid crystal shutter. A halogen lamp is used as a light source. The lamp is small enough for us to assume the lamp is a point light source. To test our method of Section 5 using real images, we separate the specular and diffuse reflection components through polarization filters [34], [15]. In order to illuminate the object with linearly polarized illuminant, a linear polarization filter is placed in front of the lamp. The experimental setup for the image acquisition system used in this experiment is illustrated in Fig. 5.

Note that color-based techniques can be also applied to separate the diffuse and specular reflection components [9], [28]. Unlike the polarization technique, the technique requires only a single image as input. However, to our knowledge, the polarization technique can most accurately separate the specular and diffuse reflection components. For this reason, we have adopted the polarization technique in our experiments.

6.1 Experiment for a Synthetic Image

This section examines the recoverability of light source position by our method of Section 4 using synthesize image. Fig. 6a shows the input synthetic image of $\boldsymbol{L} = (13, 2, 3)$. The target object in this experiment is a large board in the center of the image. By applying our method of Section 4 to this synthetic image, we obtain $\boldsymbol{L} = (12.79, 2.00, 3.00)$. Fig. 6b illustrates the image rerendered using the obtained illumination and reflectance parameters. Fig. 6c shows the error image defined as the difference between the synthesized image and the original image (red represents higher intensity compared to the original and blue lower).

6.2 Experiment for a Synthetic Specular Component Image

This section examines the recoverability of light source position by our method of Section 5 using synthetic specular component image. Fig. 7a shows the original synthetic specular component image whose source position and 3D geometric models are the same ones used in the previous experiment. We obtain $\boldsymbol{L} = (12.80, 1.99, 3.01)$.

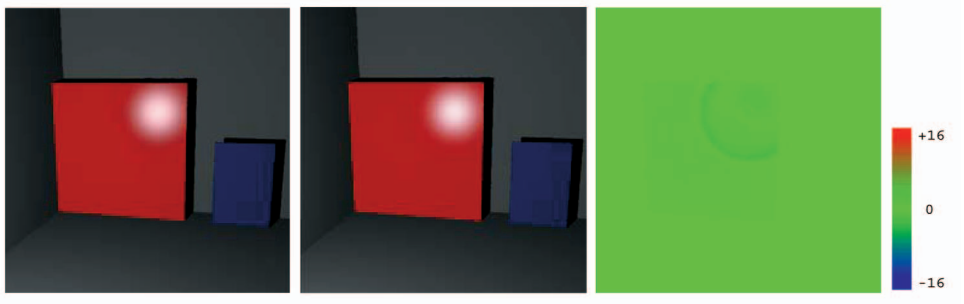

Fig. 6. Input and synthesized images: (a) input real image, (b) synthesized image, and (c) error image.

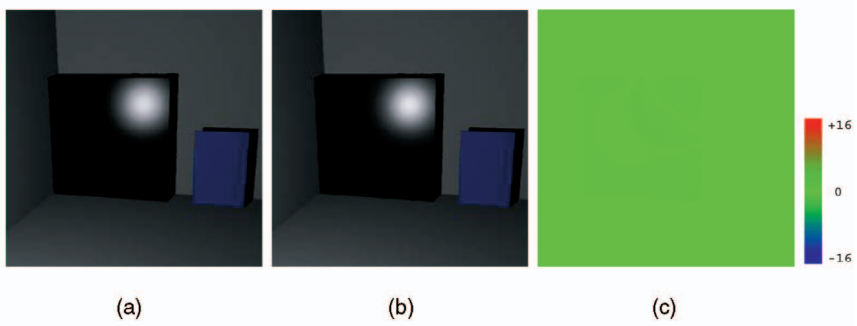

Fig. 7. Input and synthesized images: (a) input specular component image, (b) synthesized image, and (c) error image.

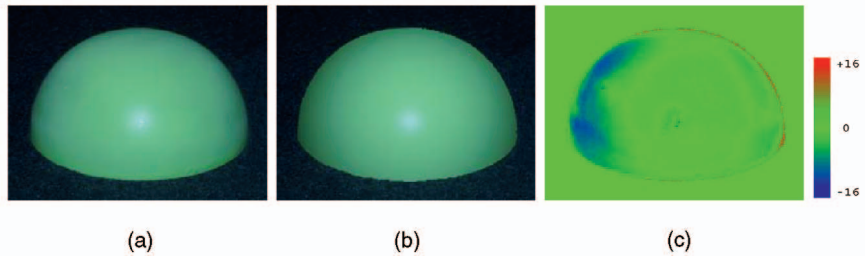

Fig. 8. Input and synthesized image: (a) input real image, (b) synthesized image, and (c) error image.

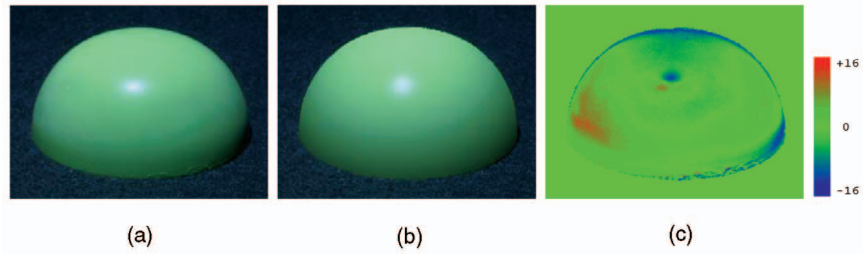

Fig. 9. Synthesized image under a new light position: (a) real image, (b) synthesized image, and (c) error image.

Fig. 7b illustrates the image calculated using the estimated illumination and reflectance parameters. Fig. 7c shows the error image defined as the difference between the synthesized image and the original specular component image.

6.3 Experiment for a Real Image

This section examines the performance of our method of Section 4 on several real images to evaluate the accuracy and stability of this method.

6.3.1 Curved Surface

Fig. 8a shows the input real image of

$$\boldsymbol{L} = (-40.88, -49.36, 80.48)\ (\mathrm{cm}).$$

We obtain

$$\begin{aligned} \boldsymbol{L} &= (-40.04, -48.83, 79.77)\ (\mathrm{cm}), \\ \tilde{K}_s &= (0.123, 0.0258, 0.249), \\ \sigma &= 0.0702, \text{and} \\ \tilde{K}_d &= (0.494, 0.840, 0.576). \end{aligned}$$

Fig. 8b shows the the synthetic image obtained using these light source and reflectance parameters. Fig. 8c shows the error image defined as the difference between the synthetic image and the original image.

Fig. 9a shows a real image of the target object captured under a different light source position from that of the above. Fig. 9b shows a synthetic image rendered under this light source position using the estimated parameters. Fig. 9c shows the error image. The main reasons why there are differences between the estimated brightness and original brightness distribution are considered as follows: 1) the input geometric model of the object has errors and 2) the surface reflection properties are not uniform over the object.

Also, we illustrate the variation of the estimates of reflection parameters (Fig. 10a) and light source position (Fig. 10b) with respect to variations of the diffuse region. The region is manually extracted at the initial stage as explained in Section 4.2. The horizontal axes in Figs. 10a and 10b represent the selected threshold value th for the diffuse region extraction. The left and right vertical axes in Fig. 10a represent $K_{d,R}$ and $(K_{s,R}, \sigma)$, respectively. The left and right vertical axes in Fig. 10b represent the z-coordinate and error of the estimates of $\boldsymbol{L}$, respectively. As can been seen in Figs. 10a and 10b, the estimates of reflection parameters and

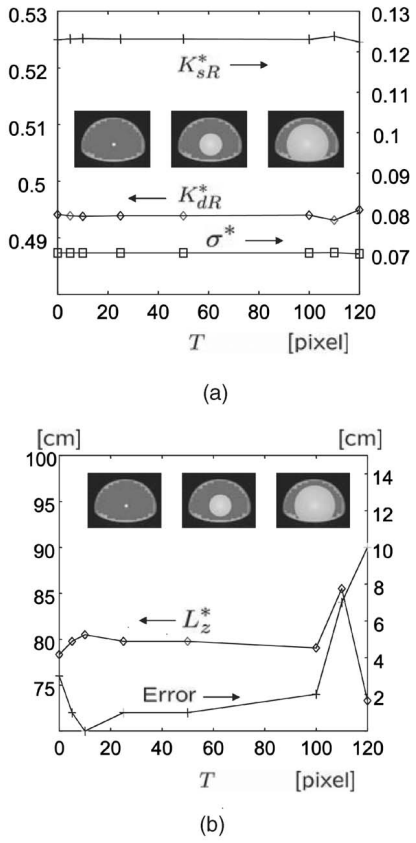

Fig. 10. Stability analysis: (a) reflectance parameter estimation and (b) light source position estimation.

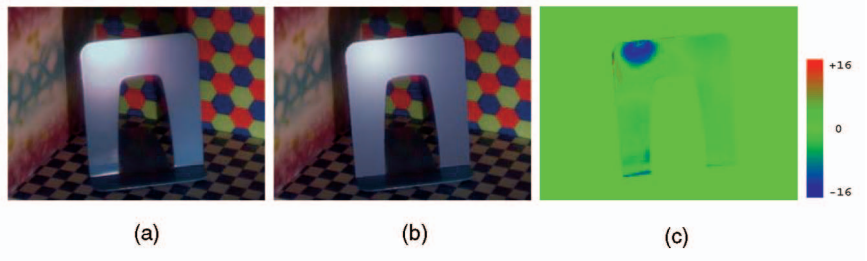

Fig. 11. Input and synthesized images: (a) input real image, (b) synthesized image, and (c) error image.

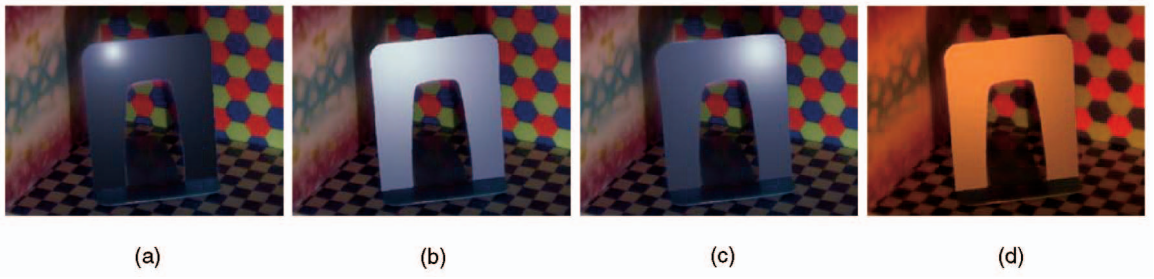

Fig. 12. Synthesized images under novel illumination conditions: (a) shorter source-surface distance, (b) longer source-surface distance, (c) different source direction, and (d) longer source-surface distance and different source color.

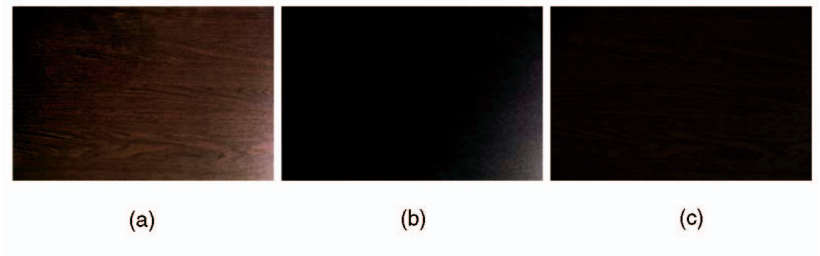

Fig. 13. Input specular component image: (a) original image, (b) specular component image, and (c) diffuse component image.

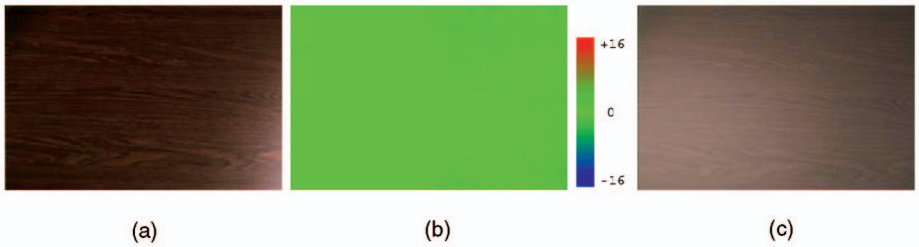

Fig. 14. Synthesized image: (a) original light position; (b) error image; (c) new light position.

the light source position are almost constant with respect to variations of the diffuse region, meaning the manual initial estimation of diffuse regions does not affect the final estimate.

6.3.2 Planar Surface

Fig. 11a shows an image of a real bookend. By applying our method of Section 4 to this color image, we obtain the synthetic image (Fig. 11b). Fig. 11c shows the error image. The apparent error (blue area) in the specular reflection area probably represents that the local search was trapped in a local minimum because the angle data α for planar surfaces may vary only relatively slightly.

Figs. 12a and 12b show the synthesized images under shorter and longer distances of light source position than that of the above, respectively. Fig. 12c shows the synthesized image under a different light source direction. Fig. 12d shows the synthesized image under a different distance and a different color (a technique that estimates illuminant color has been used [3]) of the light source.

6.4 Experiment for a Real Specular Component Image

This section examines the applicability of our method described in Section 5 to real textured surface with the uniform specular property. Also note that the specular peak is invisible. Fig. 13a shows a textured object: a poly-coated board. We apply our method of Section 4 to this object under the assumption of the perfectly uniform specular reflectance. Fig. 13b and Fig. 13c show, respectively, the specular and diffuse component images separated using polarization. Fig. 14a shows the recovered image. Fig. 14b shows the

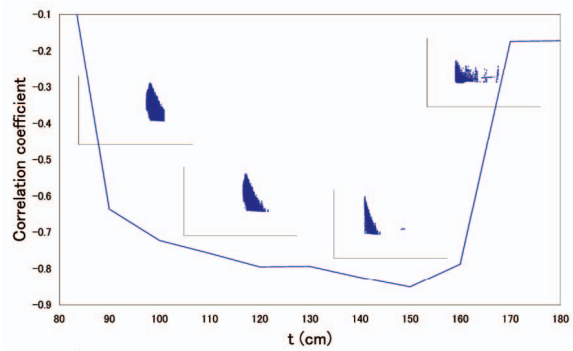

Fig. 15. Relationship between light source distance and correlation coefficient.

error image (the definition is the same as Fig. 8c) defined as the difference between the synthesized specular component image and the input specular component image (Fig. 13b). There is a minor error in Fig. 8b, which is considered due to noise in the input specular component image (the specular and diffuse reflection components are not completely and accurately separated). Fig. 14c shows the synthesized image under a different light position. Note that the diffuse reflection components are recovered by using (29). Fig. 15 shows a plot with the light source distance on the horizontal axis and the correlation coefficient (25) on the vertical axis, for a (i_p, j_p) value, in the initial estimation stage. Each graph in this figure shows a 2D plot with an X-axis and Y-axis defined in (23) and (24), respectively.

In the second-stage final estimation, we obtain $\boldsymbol{L} = (3.31, -111.51, 106.0)$ (cm), $\tilde{K}_s = (0.246, 0.297, 0.216)$, and $\sigma = 0.115$, where the ground truth for the source position is $\boldsymbol{L} = (0.0, -108.9, 99.0)$ (cm). The reasons why the estimated source position is slightly erroneous are considered as follows: 1) the target object has a transparent coat and, thus, reflection also occurs under the transparent coat and 2) the specular peak is invisible in the input image and the image pixel location of the specular peak is erroneous.

7 Conclusion

In this paper, we have presented two new methods for recovering the surface reflectance properties of an object and the light source position from a single view without the distant illumination assumption and, hence, those methods allow the image synthesis of the target object under arbitrary light source positions. In particular, the second method can also deal with textured objects with specular reflection.

The first method is done from a single real image and 3D geometric model of the object. For estimating reflectance parameters of the object stably, this method is based on the use of the iterative separating-and-fitting relaxation algorithm. Taking a specular component image as input, the second method estimates the specular reflection parameters and the light source position simultaneously by linearizing the Torrance-Sparrow specular reflection model and by optimizing the sample correlation coefficient. The first method assumes that the object has a homogeneous Lambertian diffuse reflection property. The second method does not require these assumptions and, thus, can handle diffuse textured and non-Lambertian objects; however, it is less robust than the first method because no information about diffuse reflection is available.

We have empirically found that the algorithm converges and, in all experiments, it converged to a plausible minima. However, a rigorous analysis on its convergence characteristics is left as future work. Note that we need to know the surface normals of the object in the image. This can be provided by using various techniques including, for

TABLE 1
List of Symbols

c	R, G and B component
I_c	Image pixel value in each c
θ_i	Angle between light source direction and the surface normal
θ_r	Angle between viewing direction and surface normal
α	Angle between surface normal and bisector of viewing direction and light source direction
$L_{q,c}$	Radiance of point light source in c
r	Distance between point light source and surface point
L_c	$L_{q,c}$ divided by r^2
$k_{d,c}$	Coefficients for diffuse component
$k_{s,c}$	Coefficients for specular component
σ	Surface roughness
$K_{d,c}$	$k_{d,c}$ multiplied by $L_{q,c}$
$K_{s,c}$	$k_{s,c}$ multiplied by $L_{q,c}$
P	Surface point satisfying $\alpha = 0$
$\boldsymbol{L}_p$	Unit vector with a light source direction and a starting point P
$\boldsymbol{V}_p$	Unit vector with a viewing direction and a starting point P
$\boldsymbol{N}_p$	Unit normal vector at P
$\boldsymbol{L}$	Location vector of light source
$\boldsymbol{P}$	Location vector of P
t	Light source distance (Distance between $\boldsymbol{P}$ and $\boldsymbol{L}$)
(i_p, j_p)	Pixel location of specular peak
Ω_d	Set of 2D points of diffuse region
Ω	Set of 2D points of object's surface
T	Integer concerning radius of specular region
N_d	Number of 2D points in Ω_d
$I(i,j)$	Pixel value observed at 2D point (i,j)
$u(i,j,t)$	$I(i,j)$ divided by $\cos\theta_i / r^2$ under t
$r(i,j,t)$	Distance between light source and surface point (i,j) under t
t^*, t^+	Solutions of t in 1st and 2nd methods
Ω_t	Solution space of t
t_{min}, t_{max}	Lower and upper bounds of t
Δt	Step length of t
K_d^*, K_d^+	Solutions of K_d in 1st and 2nd methods
$I_s^*(i,j)$, $I_d^*(i,j)$	Separated specular and diffuse images during iteration
$(x(i,j),\ y(i,j))$	Set of data pairs by logarithm transformation of specular term
a, b	Slope and Y-intercept of fitted line to $(x(i,j), y(i,j))$
γ	Step size in iteration of σ
$\mu^{(l)}$	Intermediate variable of σ
K_s^*, K_s^+	Solutions of K_s in 1st and 2nd methods
σ^*, σ^+	Solutions of σ in 1st and 2nd methods
I_d, I_s	Diffuse and specular reflection component
$(X(i,j,p,t), Y(i,j,p,t))$	Set of data pairs by logarithm transformation of specular term under p and t values
Ω_p	Solution space of p
p^+	Solution of p
$\overline{X}(p,t)$, $\overline{Y}(p,t)$	Sample means of X and Y
N	Number of 2D points belonging to Ω
$K_d^+(i,j)$	Diffuse parameter value of (i,j)

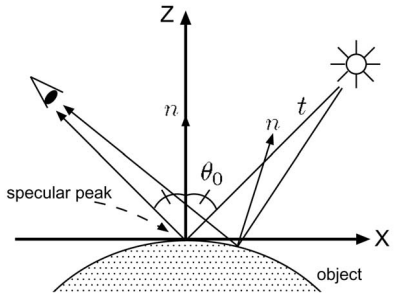

Fig. 16. Geometric model.

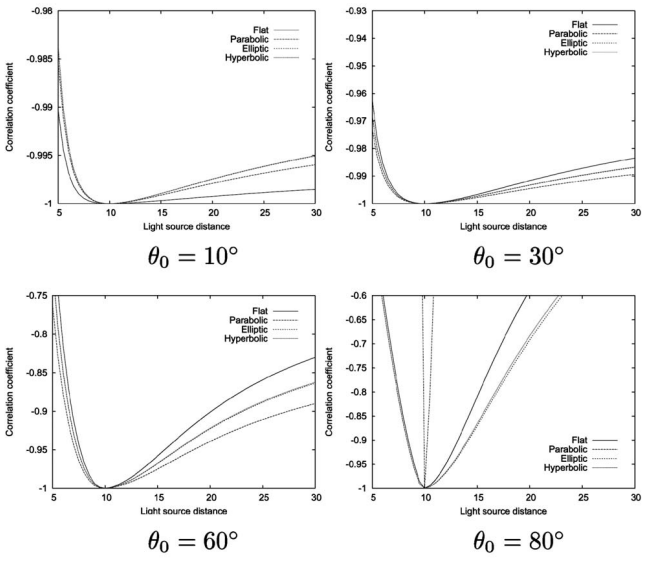

Fig. 17. Correlation coefficient with respect to variations of the light source distance for different θ_0 (no noise added).

instance, shape-from-shading [4], [6], [2], [35], [12]. In this paper, we simply used a light stripe range finder to obtain the range image of the scene. Since the same camera is used to capture both the range image and the color image, each pixel in the color image will have 3D coordinates assigned to it. Hence, the surface normal can be easily computed per pixel. Although assuming preacquired 3D geometry would sound restrictive, given the recent advance and wide use of accurate range finders, we believe this assumption does not lessen the applicability of our framework in practical scenarios. We intend to extend the current method to the cases of erroneous geometric models in future work.

Appendix A

List of Symbols

The symbols used in the paper are listed in Table 1.

Appendix B

Uniqueness and Stability of Light Source Distance

In this section, we analyze local uniqueness and stability of the solutions of (25) using simulation. As shown in Fig. 16, the xyz-coordinate system is arranged so that the origin is at the specular peak and the z-axis is parallel to the surface

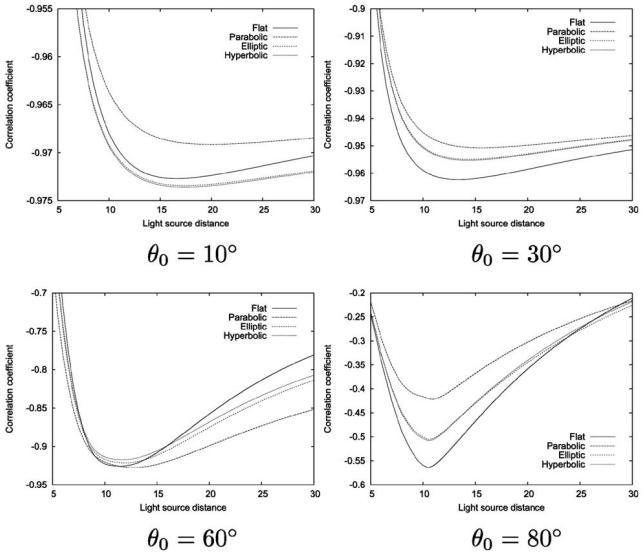

Fig. 18. Correlation coefficient with respect to variations of the light source distance for different θ_0 (Gaussian noise $N(0, 5^2)$ added to the intensities of the pixels).

normal. The four graphs in Fig. 17 show the correlation coefficients (25) (the values are computed using (4)) with respect to variations of the light source distance t for different angles θ_0. The four curves in each graph correspond to a planar surface ($z = 0$), a parabolic one ($x^2 + y^2 + 16z = 0$), an elliptic one ($x^2 + y^2 + 16(z+1)^2 = 16$), and a hyperbolic one ($x^2 + y^2 - 16(z-1)^2 = -16$), respectively. Also, the four graphs in Fig. 18 show the correlation coefficients (25) for the intensities of the pixels that have been corrupt with Gaussian noise with mean 0 and standard deviation 5 for different angles θ_0. Fig. 17 and Fig. 18 show that the light source distance can be uniquely determined for flat or quadratic surfaces and that the solutions can be found more stably for the larger values of θ_0.

Acknowledgments

The work described in this paper is, in part, supported by Japan Science and Technology (JST) under CREST Ikeuchi Project.

References

[1] S. Boivin and A. Gagalowicz, "Image-Based Rendering of Diffuse, Specular and Glossy Surfaces from a Single Image," *Proc. SIGGRAPH Conf.*, pp. 197-216, 2001.

[2] M.J. Brooks and B.K.P. Horn, "Shape and Source from Shading," *Proc. Int'l Joint Conf. Artificial Intelligence*, pp. 932-936, 1985.

[3] G.D. Finlayson and G. Schaefer, "Solving for Color Constancy Using Constrained Dichromatic Reflection Model," *Int'l J. Computer Vision*, vol. 42, no. 3, pp. 127-144, 2001.

[4] B. Horn and M. Brooks, *Shape from Shading*. Cambridge, Mass.: MIT Press, 1989.

[5] D.R. Hougen and N. Ahuja, "Estimation of the Light Source Distribution and Its Use in Integrated Shape Recovery from Stereo Shading," *Proc. IEEE Int'l Conf. Computer Vision*, pp. 148-155, 1993.

[6] K. Ikeuchi and B.K.P. Horn, "Numerical Shape for Shading and Occluding Boundaries," *Artificial Intelligence*, vol. 17, nos. 1-3, pp. 141-184, 1981.

[7] K. Ikeuchi and K. Sato, "Determining Reflectance Properties of an Object Using Range and Brightness Images," *IEEE Trans. Pattern Analysis and Machine Intelligence*, vol. 13, no. 11, pp. 1139-1153, 1991.

[8] C.-Y. Kim, A.P. Petrov, H.-K. Choh, Y.-S. Seo, and I.-S. Kweon, "Illuminant Direction and Shape of a Bump," *J. Optical Soc. Am.,* vol. 15, no. 9, pp. 2341-2350, 1998.
[9] G.J. Klinker, S.A. Shafer, and T. Kanade, "Using a Color Reflection Model to Separate Highlights from Object Color," *Proc. IEEE Int'l Conf. Computer Vision,* pp. 145-150, 1987.
[10] Y. Li, S. Lin, H. Lu, and H. Shum, "Multiple-Cue Illumination Estimation in Textured Scenes," *Proc. IEEE Int'l Conf. Computer Vision,* pp. 1366-1373, 2003.
[11] S.R. Marschner and D.P. Greenberg, "Inverse Lighting for Photography," *Proc. Fifth Color Imaging Conf.,* Soc. Imaging Science and Technology, pp. 262-265, 1997.
[12] D. Miyazaki, R.T. Tan, K. Hara, and K. Ikeuchi, "Polarization-Based Inverse Rendering from a Single View," *Proc. IEEE Int'l Conf. Computer Vision,* pp. 982-987, 2003.
[13] N. Mukawa, "Estimation of Shape, Reflection Coefficients and Illuminant Direction from Image Sequences," *Proc. IEEE Int'l Conf. Computer Vision,* pp. 507-512, 1990.
[14] S.K. Nayar, K. Ikeuchi, and T. Kanade, "Surface Reflection: Physical and Geometrical Perspectives," *IEEE Trans. Pattern Analysis and Machine Intelligence,* vol. 13, no. 7, pp. 611-634, 1991.
[15] S.K. Nayar, X. Fang, and T.E. Boult, "Removal of Specularities Using Color and Polarization," *Proc. Computer Vision and Pattern Recognition,* pp. 583-590, 1993.
[16] K. Nishino, Z. Zhang, and K. Ikeuchi, "Determining Reflectance Parameters and Illumination Distribution from a Sparse Set of Images for View-Dependent Image Synthesis," *Proc. IEEE Int'l Conf. Computer Vision,* pp. 599-606, 2001.
[17] K. Nishino, "Photometric Object Modeling—Rendering from a Dense/Sparse Set of Images—," PhD thesis, The Univ. of Tokyo, 2002.
[18] T. Okatani and K. Deguchi, "Shape Reconstruction from an Endoscope Image by Shape from Shading Technique for a Point Light Source at the Projection Center," *Computer Vision and Image Understanding,* vol. 66, no. 2, pp. 119-131, 1997.
[19] A.P. Pentland, "Finding the Illuminant Direction," *J. Optical Soc. Am.,* vol. 72, pp. 448-455, 1982.
[20] http://radsite.lbl.gov/radiance/HOME.html, 1997.
[21] R. Ramamoorthi and P. Hanrahan, "Analysis of Planar Light Fields from Homogeneous Convex Curved Surfaces under Distant Illumination," *Proc. SPIE, Human Vision and Electronic Imaging VI,* pp. 185-198, 2001.
[22] R. Ramamoorthi and P. Hanrahan, "A Signal Processing Framework for Inverse Rendering," *Proc. SIGGRAPH Conf.,* pp. 117-128, 2001.
[23] I. Sato, Y. Sato, and K. Ikeuchi, "Acquiring a Radiance Distribution to Superimpose Virtual Objects onto a Real Scene," *Proc Int'l Assoc. Pattern Recognition Workshop Machine Vision Applications,* pp. 19-22, 1998.
[24] I. Sato, Y. Sato, and K. Ikeuchi, "Ilumination Distribution from Shadows," *Proc. IEEE Conf. Computer Vision and Pattern Recogition,* pp. 306-312, 1999.
[25] I. Sato, Y. Sato, and K. Ikeuchi, "Illumination Distribution from Brightness in Shadows: Adaptive Estimation of Illumination Distribution with Unknown Reflectance Properties in Shadow Regions," *Proc. IEEE Int'l Conf. Computer Vision,* pp. 875-882, 1999.
[26] Y. Sato, M. Wheeler, and K. Ikeuchi, "Object Shape and Reflectance Modeling from Observation," *Proc. SIGGRAPH,* pp. 379-387, 1997.
[27] S. Shafer, "Using Color to Separate Reflection Components," *COLOR Research and Application,* vol. 10, pp. 210-218, 1985.
[28] R.T. Tan, K. Nishino, and K. Ikeuchi, "Separating Diffuse and Specular Reflection Components Based on Surface Color Ratio and Chromaticity," *Proc. Int'l Assoc. Pattern Recognition Workshop Machine Vision Applications,* pp. 14-19, 2002.
[29] S. Tominaga and N. Tanaka, "Estimating Reflection Parameters from a Single Color Image," *IEEE Computer Graphics and Applications,* vol. 20, no. 5, pp. 58-66, 2000.
[30] K.E. Torrance and E.M. Sparrow, "Theory of Off-Specular Reflection from Roughened Surfaces," *J. Optical Soc. Am.,* vol. 57, pp. 1105–1114, 1967.
[31] Y. Wang and D. Samaras, "Estimation of Multiple Illuminants from a Single Image of Arbitrary Known Geometry," *Proc. European Conf. Computer Vision,* pp. 272-288, 2002.
[32] Y. Wang and D. Samaras, "Estimation of Multiple Directional Light Sources for Synthesis of Augmented Reality Images," *Graphical Models,* vol. 65, no. 4, pp. 185-205, 2003.
[33] G.J. Ward, "Measuring and Modeling Anisotoropic Reflection," *Proc. SIGGRAPH Conf.,* pp. 265-272, 1992.
[34] L.B. Wolff and T.E. Boult, "Constraining Object Features Using a Polarization Reflectance Model," *IEEE Trans. Pattern Analysis and Machine Intelligence,* vol. 13, no. 6, pp. 167-189, 1991.
[35] Y. Yang and A. Yuille, "Source from Shading," *Proc. IEEE Conf. Computer Vision and Pattern Recogition,* pp. 534-539, 1991.
[36] Y. Zhang and Y.H. Yang, "Multiple Illuminant Direction Detection with Application to Image Synthesis," *IEEE Trans. Pattern Analysis and Machine Intelligence,* vol. 23, no. 8, pp. 915-920, 2001.
[37] Q. Zheng and R. Chellappa, "Estimation of Illuminant Direction, Albedo, and Shape from Shading," *IEEE Trans. Pattern Analysis and Machine Intelligence,* vol. 13, no. 7, pp. 680-702, 1991.

Kenji Hara received the BE and ME degrees from Kyoto University in 1987 and 1989, respectively. He then held several positions at Takeda Pharmaceutical Co., Ltd. and Fukuoka Industrial Technology Center, Japan. He received the PhD degree from Kyushu University in 1999. Since 2001, he has been an adjunctive researcher at The University of Tokyo. In 2004, he joined Kyushu University, where he is currently an associate professor in the Department of Visual Communication Design. His research interests include physics-based vision and geometric modeling. He is a member of the IEEE.

Ko Nishino received the BE and ME degrees from The University of Tokyo in 1997 and 1999, respectively. He received the PhD degree in information science from The University of Tokyo in 2002. Since 2002, he has been a postdoctoral research scientist at Columbia University. His research interests span computer vision and computer graphics. He has published papers on photometric and geometric problems in scene and object modeling that include physics-based vision, image-based modeling and rendering. He is a member of the IEEE and ACM.

Katsushi Ikeuchi received the BE degree from Kyoto University in 1973 and the PhD degree from the University of Tokyo in 1978. After working at the Artificial Intelligence Laboratory, MIT, for three years, the Electrotechnical Laboratory, MITI, for five years, and the School of Computer Science, Carnegie Mellon University, for 10 years, he joined the University of Tokyo in 1996 and is currently a full professor. His research interest spans computer vision, robotics, and computer graphics. In these research fields, he has received several awards, including the David Marr Prize in computational vision for the paper "Shape from Interreflection" and IEEE R&A K-S Fu memorial best transaction paper award for the paper "Toward Automatic Robot Instruction from Perception–Mapping Human Grasps to Manipulator Grasps." In addition, in 1992, his paper, "Numerical Shape from Shading and Occluding Boundaries," was selected as one of the most influential papers to have appeared in the *Artificial Intelligence Journal* within the past 10 years. His IEEE activities include general chair, IROS95, ITSC00, IV01; program chair, CVPR96, ICCV03; associate editor, IEEE *TRA*, IEEE *TPAMI*; and distinguished lecturer SPS (2000-2002), RAS (2004-2006). Dr. Ikeuchi is a member of the Computer Society and was elected as an IEEE fellow in 1998. He is also the EIC of the *International Journal of Computer Vision*.